Available online at www.sciencedirect.com
SCIENCE DIRECT®
PERGAMON
International Journal of Heat and Mass Transfer 46 (2003) 1371–1383
International Journal of HEAT and MASS TRANSFER
www.elsevier.com/locate/ijhmt

Stability analysis for three-dimensional Rayleigh–Bénard convection with radiatively participating medium using spectral methods

C.H. Lan, O.A. Ezekoye, J.R. Howell *, K.S. Ball

Department of Mechanical Engineering, The University of Texas at Austin, Austin, TX 78712, USA

Received 28 March 2002; received in revised form 27 September 2002

Abstract

In this study, a fluid subject to combined natural convection and radiation is studied by employing the Boussinesq approximation of the Navier–Stokes equations. The solution for the flow field within a three-dimensional rectangular enclosure is found numerically using a spectral method. The equation of radiation transfer for the participating medium is analyzed by the exact integral formulation. Black boundaries and a gray medium are prescribed. Linear stability analysis and weakly nonlinear analysis are used to determine the critical Rayleigh number for the onset of convection in the combined mode. For the system with flow, a modified second-order time splitting method and a spectral collocation method are introduced to minimize the errors in the computation. From numerical simulation and stability analysis, insight into the effect of radiation on this classical problem can be accomplished. The results show that the presence of a radiative source changes the static temperature gradient of the fluid, and generally results in increasing the flow critical values. The influences of the conduction–radiation parameter, Rayleigh number, and optical thickness on flow instabilities and bifurcations are discussed.

1. Introduction

For the past century, Rayleigh–Bénard convection has been studied extensively using theoretical, experimental and numerical approaches. The effect of radiation on the flow is of interest because of its importance in the fundamental understanding of heat transfer in natural convection and in practical applications. These applications include energy systems such as solar collectors, furnaces, heat exchangers and many energy storage devices; manufacturing processes such as crystal growth and processing of silicon wafers; and natural phenomena such as the spread of fire. For radiative heat transfer problems, if heat convection occurs simultaneously, there are mathematical complications in addition to those encountered in the pure radiation case. For combined-mode problems, the conventional linear stability theory to predict the critical Rayleigh number becomes more complicated. In this study, a linear stability analysis, a weakly nonlinear stability analysis, a direct numerical simulation of the full three-dimensional combined-mode problem, and experimental work reported in the literature are applied to obtain insight into the effect of radiation on this classical problem.

For the analytical model, Goody [1] applied linear stability theory to determine the critical Rayleigh number for the limiting cases of optically thin and thick media bounded by free surfaces. Following Goody, Spiegel [2] treated the same problem with a wide range of optical thickness and for black rigid bounding surfaces; Christophorides and Davis [3] included the effect of a nonlinear initial temperature; Arpaci and Gozum [4] treated a nongray fluid and boundaries by the Eddington approximation; Lienhard [5] expanded a single layer instability to a coupled layer instability with boundary radiation; Yang [6] examined the instability of radiation-induced flow in an inclined slot with one side heated by

* Corresponding author. Tel.: +1-512-471-3095; fax: +1-512-471-1045.
E-mail address: jhowell@mail.utexas.edu (J.R. Howell).

0017-9310/03/$ - see front matter © 2002 Elsevier Science Ltd. All rights reserved.
PII: S0017-9310(02)00422-2

Nomenclature

$A_{1,2}$	aspect ratio; $A_1 = L_x/L_z$, $A_2 = L_y/L_z$
a	absorption coefficient, m^{-1}
c_p	specific heat, kJ/(kg K)
D	derivative of z-direction
E_n	exponential integral functions of order n
K	extinction coefficient, $(a + \sigma_s)$, m^{-1}
k	wave number
$L_{x,y,z}$	spatial length in the enclosure, m
N	conduction–radiation parameter, $a\kappa/4\sigma\overline{T}^3$
Nu	the average Nusselt number
P	nondimensional pressure
p	the growth rate of disturbances
Pr	Prandtl number, v/α
Q_r	the average nondimensional radiative heat flux, defined in Eq. (29)
Q_t	the average nondimensional total heat flux, defined in Eq. (30)
q_c	local nondimensional conductive heat flux
q_r	local nondimensional radiative heat flux
q_t	local nondimensional total heat flux
Ra	Rayleigh number, $g\beta(T_h - T_c)L^3/v\alpha$
$T_{m,n}$	Chebyshev polynomials
$\overline{T}$	the mean temperature, K
t	nondimensional time
$\overline{V}$	intermediate velocity
W	linearized velocity disturbance function
u, v, w	nondimensional velocity components
x, y, z	coordinates

Greek symbols

α	thermal diffusivity, m^2/s
β	volumetric coefficient of expansion, K^{-1}
γ	temperature gradient, dT/dz
ε	nondimensional amplitude of perturbation
κ	thermal conductivity, W/(m K)
v	kinematic viscosity, m^2/s
Θ	linearized temperature disturbance function
θ	nondimensional temperature
ρ	density, kg/m^3
σ	Stefan–Boltzmann constant, 5.67×10^{-8} W/(m^2 K^4)
σ_s	scattering coefficient, m^{-1}
τ	optical thickness, $= az$
χ	nondimensional radiation-conductivity, $16\sigma\overline{T}^3/\ 3a\kappa$

Subscripts

c	conductive heat transfer; critical values; cold wall
h	hot wall
r	radiative heat transfer
s	stationary state
t	total heat transfer

Superscripts

$n-1$, n, $n+1$	previous, current, and next time levels

an external source; Bdéoui and Soufiani [7] analyzed the onset of Rayleigh–Bénard instability for real molecular emitting and absorbing gases using the full integro-differential formulation.

Experimental studies of the radiative effects on Rayleigh–Bénard convection have also been examined. Gille and Goody [8] conducted the first experimental study of the effect of radiative transfer on the onset of Rayleigh–Bénard convection by comparing data for dry air and NH_3 between parallel aluminum plates maintained at different temperatures. Their experiments indicated that the critical Rayleigh number in NH_3 is greatly increased over the critical values for air. Hutchison and Richards [9] experimentally determined the onset of Rayleigh–Bénard convection in a radiatively participating gas by comparing air to mixtures of air and CO_2, and CO_2 only and revealed about a 7–20% increase in critical Rayleigh number in the radiatively participating gas. For nonradiative flow, there are numerous papers on the topic, and Maveety and Leith [10] performed recent experimental investigations of heat flux characteristics for air within moderate size containers with different aspect ratios.

For the present direct numerical simulation, modified second-order time splitting methods coupled with a high order accurate Chebyshev–Fourier spectral collocation technique are applied to solve two-dimensional and three-dimensional governing equations. The pressure gradient is decoupled from the momentum equation, a Poisson equation is solved for a scalar potential, and the velocities are corrected to satisfy the continuity constraint [11]. Spectral methods involve seeking the solutions to differential equations in terms of a series of known smooth functions; usually these are orthogonal polynomials such as Fourier series and Chebyshev polynomials [12]. The use of spectral methods to simulate transport phenomena in fluid mechanics is a promising alternative to more traditional finite-difference or finite element techniques, due to the high accuracy and fast convergence with increasing resolution. Kuo et al. [13] studied the combined natural convection and radiation in a two-dimensional horizontal annulus filled with a radiatively participating gray medium using spectral collocation methods coupled with an influence matrix technique. An unusual flow structure and multiple solutions are found, including a more realistic

steady-state solution compared to those from control volume based finite-difference methods. In the present work, the Chebyshev collocation method is used for evaluating spatial derivatives and the Chebyshev–Gauss quadrature for evaluating the spatial integrations. The matrix diagonalization technique by Haidvogel and Zang [14] is used to solve the matrix equation resulting from spectral discretization. For combined radiation-convection, the incompressible Navier–Stokes equations in primitive variable formulation are solved under the Boussinesq approximation. A modified time splitting technique [15] with prescribed velocity and pressure boundary conditions is applied to satisfy continuity.

The purposes of this work are (i) to develop the spectral method to include the exact integral formulation of radiative heat transfer, providing an alternative numerical method for radiation heat transfer studies; (ii) to present the effects of radiative heat transfer on natural convection in three-dimensional participating media; (iii) to compare the results of the linear analysis and the direct numerical simulation with existing experimental results. These solutions provide benchmarks for researchers in the radiative heat transfer field and also provide definitive solutions that demonstrate the effect of the radiation transfer on the critical Rayleigh number in an enclosure with participating media. The influence of the conduction–radiation parameter, Rayleigh number and optical thickness on flow instabilities and bifurcations is discussed.

The results with radiation are limited to the case of a gray gas. This approximation is poor if large temperature differences are present within the enclosure. For small temperature differences typical of many natural convection problems, the results for gray gas radiation illustrate the trends expected for the more exact nongray case.

2. Formulation and numerical methods

Consider a viscous fluid of density ρ which varies according to the Boussinesq approximation, and which has constant and uniform thermal conductivity κ, specific heat c_p, and coefficient of thermal expansion β and is enclosed in a rectangular three-dimensional enclosure. The radiatively participating medium is gray, with linear absorption coefficient a, and all boundaries are black. The distance between a top and bottom boundary surface is L. The two geometries studied are shown in Fig. 1. The linear analysis is applied to two unlimited parallel plates, and the direct simulation is applied to a three-dimensional rectangular enclosure. The lower and upper walls are isothermal, $T_h > T_c$, and the average temperature $\overline{T} = (T_h + T_c)/2$, is used as the reference temperature. The governing conservation relations are:

$$\nabla \cdot \vec{u} = 0 \tag{1}$$

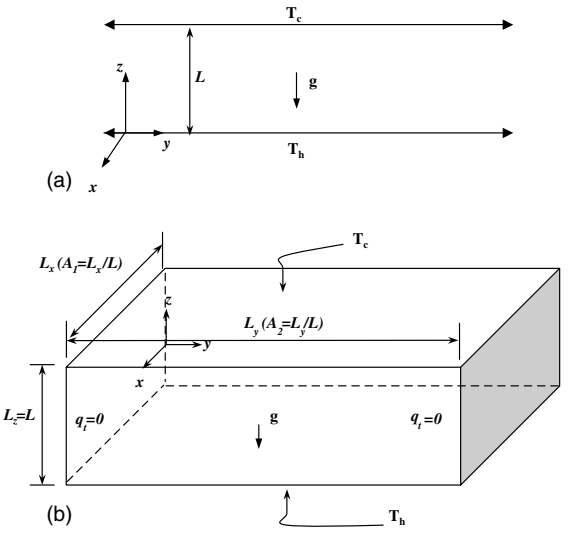

Fig. 1. (a) The geometry for the linear analysis; (b) The geometry for direct numerical simulations.

$$\frac{\partial \vec{u}}{\partial t} + (\vec{u} \cdot \nabla \vec{u}) = -\frac{1}{\rho}\nabla P + \vec{g}\beta(T - \overline{T}) + \nu \nabla^2 \vec{u} \tag{2}$$

$$\frac{\partial T}{\partial t} + \vec{u} \cdot \nabla T = \frac{\kappa}{\rho c_p}\left(\nabla^2 T - \frac{1}{\kappa}\nabla \cdot q_r\right) \tag{3}$$

In Eq. (3), $\nabla \cdot q_r$ is the divergence of radiative flux, and can be expressed as

$$\nabla \cdot q_r = 4a\sigma T^4(\vec{r}) - a\left\{\int_A i'(T(\vec{r}_0);\vec{r}_0)\frac{\hat{n}\cdot(\vec{r}-\vec{r}_0)}{|\vec{r}-\vec{r}_0|^3}e^{-K(|\vec{r}-\vec{r}_0|)}\,dA + K\int_V \frac{I'(T(\vec{r}^*);\vec{r}^*)e^{-K(|\vec{r}-\vec{r}^*|)}}{|\vec{r}-\vec{r}^*|^2}\,dV^*\right\} \tag{4}$$

for an isotropically scattering participating medium with uniform properties [16].

2.1. Linear stability analysis

The linear stability theorem describes the reaction of the fluid to infinitesimal perturbations of the basic steady state. Following Chandrasekhar [17], the basic state of the system is the stationary state, $\vec{u} = 0$, and in this state

$$\nabla P_s = \rho \vec{g}\beta(T_s - \overline{T}) \tag{5}$$

$$\kappa \nabla^2 T_s = \nabla \cdot q_{rs} \tag{6}$$

In this reference state, we assume that P_s and T_s vary only along the z vertical direction.

$$P_s = P_0 + \rho g\beta(T_s - \overline{T})z \tag{7}$$

$$\kappa\frac{\partial^2 T_s}{\partial z^2} = 4a\sigma T_s^4 - 2a\sigma\left[T_h^4 E_2(\tau) + T_c^4 E_2(\tau_D - \tau) + \int_0^{\tau_D} T_s^4 E_1(|\tau - \tau^*|)\,d\tau^*\right] \tag{8}$$

where E_1, E_2 and E_3 are the exponential integral functions.

The local total heat flux q_{ts} in the z-direction is assumed to be constant, and expressed as:

$$q_{ts} = q_{cs} + q_{rs} \tag{9a}$$

$$q_{ts} = -\kappa\left.\frac{dT_s}{dz}\right|_{z=0} + \sigma T_h^4 - 2\sigma T_c^4 E_3(\tau_D) - 2\int_0^{\tau_D}\sigma T_s^4(\tau^*)E_2(\tau^*)\,d\tau^* \tag{9b}$$

In linear stability analysis, without a radiative effect the gradient of temperature is constant, $dT_{cs}/dz = \Delta T/d = \gamma_0$. For the combined-mode problem, the gradient of temperature will vary:

$$\frac{dT_s}{dz} = -\gamma(z) \tag{10}$$

We now study the effect of perturbations on the system around the above specified reference state. By taking the double curl of the momentum equations and keeping only the vertical component of the velocity, δw, and introducing dimensionless scales as:

$$x_i^* = x_i/L, \quad t^* = t\Big/\left(\frac{L^2}{\alpha}\right), \quad \theta^* = \delta\theta\Big/\left(\frac{v\alpha}{g\beta L^3}\right),$$
$$w^* = \delta w\Big/\left(\frac{\alpha}{L}\right), \quad P^* = \delta P\Big/\left(\frac{\rho v\alpha}{L^2}\right)$$

the governing equations become:

$$\frac{\partial\nabla^2 w^*}{\partial t^*} = Pr\left(\frac{\partial^2\theta^*}{\partial x^{*2}} + \frac{\partial^2\theta^*}{\partial y^{*2}} + \nabla^4 w^*\right) \tag{11}$$

$$\frac{\partial\theta^*}{\partial t^*} - Ra\frac{\gamma(z)}{\gamma_0}w^* = \nabla^2\theta^* - \frac{\tau_D^2}{N}\nabla\cdot q_r^* \tag{12}$$

$$\nabla\cdot q_r^* = \left\{4\theta^* - \left[\int_0^{\tau_D}(2\theta^*)E_1(|\tau - \tau^*|)\,d\tau^*\right]\right\} \tag{13}$$

where the dimensionless parameters are

$$N = \frac{\kappa a}{4\sigma\overline{T}^3}, \quad Ra = \frac{g\beta(T_h - T_c)L^3}{v\alpha}, \quad Pr = \frac{v}{\alpha} \tag{14}$$

For convenience, we shall drop the asterisk on the nondimensional variables and deal with nondimensional equations only. The perturbed quantities can be written in the form

$$w = W(z)\exp[i(k_x x + k_y y) + pt] \tag{15a}$$

$$\theta = \Theta(z)\exp[i(k_x x + k_y y) + pt] \tag{15b}$$

where k_x and k_y are the wave numbers of the disturbances in the x- and y-directions, and p is the growth rate of the disturbances. Letting $D = \partial/\partial z$, and $k = (k_x^2 + k_y^2)^{1/2}$, we obtain

$$\frac{p}{Pr}(D^2 - k^2)W = -k^2\Theta + (D^2 - k^2)^2 W \tag{16}$$

$$p\Theta = Ra\frac{\gamma(z)}{\gamma_0}W + (D^2 - k^2)\Theta - \frac{\tau_D^2}{N}\nabla\cdot q_r \tag{17}$$

On a rigid boundary, the no-slip condition requires velocity components to vanish. From the continuity equation it follows that $DW = 0$ at the boundary. The temperature disturbance is also required to disappear at the boundary. We thus have the boundary conditions:

$$DW = 0, \quad W = \Theta = 0 \quad \text{for } z = 0, 1 \tag{18}$$

The marginal states are characterized by $p = 0$. Therefore, we obtain

$$(D^2 - k^2)^2 W = k^2\Theta \tag{19}$$

$$Ra\frac{\gamma(z)}{\gamma_0}W = -(D^2 - k^2)\Theta + \frac{\tau_D^2}{N}\nabla\cdot q_r \tag{20}$$

Eqs. (19) and (20) with boundary conditions (18) construct an eigenvalue problem, which is solved numerically using a Chebyshev collocation method. For nontrivial solutions, the real part of the most unstable eigenvalue vanishes at a neutral state. The critical stability values can be found analytically in the pure convective case, but not in the combined radiative heat transfer case.

The divergence of radiative flux $\nabla\cdot q_r$ is evaluated iteratively using a pseudospectral method [18]. The calculations are continued until the real part of the most unstable eigenvalue is less than 10^{-6} and changes in the solution are less than 0.1% at any point. We can find the eigenvalues very accurately, if the spectral approximation converges rapidly. For the fixed parameters, different Ra at the marginally stable state may be obtained for different wave numbers. The minimum Rayleigh number is called the critical Rayleigh number, which occurs at the critical wave number k.

2.2. Direct numerical simulation

For the direct numerical simulation, the same dimensionless scales are introduced as those in the linear analysis, except that $\theta = T/\overline{T}$. The governing equations in nondimensional form are:

$$\nabla\cdot\vec{u} = 0 \tag{21}$$

$$\frac{\partial\vec{u}}{\partial t} + \vec{u}\cdot(\nabla\vec{u}) = Pr\left[-\nabla P + \nabla^2\vec{u} + Ra\frac{(\theta - 1)}{(\theta_h - \theta_c)}\right] \tag{22}$$

$$\frac{\partial\theta}{\partial t}+\vec{u}\cdot(\nabla\theta)=\nabla^2\theta-\frac{\tau_D^2}{N}\nabla\cdot q_r \tag{23}$$

To solve the governing equations, velocity, pressure, and temperature boundary conditions are required. In the direct numerical simulations, we assume that all physical variables in the x-direction are 2π-periodic, and in the y- and z-directions are nonperiodic. $A_1=2\pi/L$ and $A_2=L_y/L$ are the aspect ratios of the computational box in the x- and y-directions, respectively. The nonperiodic boundary conditions are:

$$u,v,w=0 \quad \text{at } z=\pm1 \quad \text{and} \quad y=\pm A_2 \tag{24}$$

$$\theta=\theta_h \quad \text{and} \quad \theta=\theta_c \quad \text{at } z=-1 \quad \text{and} \quad z=1, \text{ respectively} \tag{25}$$

$$\frac{\partial\theta}{\partial y}=\frac{\tau_D}{N}q_r \quad \text{at } y=\pm A_2 \tag{26}$$

The local nondimensional heat flux at $z=\pm1$ is defined as:

$$q_t|_{z=\pm1}=\left.\frac{q_r}{4N}\right|_{z=\pm1}-\nabla\theta|_{z=\pm1} \tag{27}$$

On the right hand side of Eq. (27), the first term is the nondimensional radiative heat flux, and the second term is the nondimensional temperature gradient equivalent to the nondimensional conductive heat flux. At the top and bottom walls, the definition of the average Nusselt number is:

$$Nu=\frac{Nu|_{z=1}+Nu|_{z=-1}}{2},$$
$$Nu|_{z=\pm1}=\left|\int_{-A_2}^{A_2}\int_0^{A_1}\frac{\partial\theta}{\partial z}\,dx\,dy\right|_{z=\pm1} \tag{28}$$

In order to make quantitative comparisons with pure convection problems, the average radiative heat flux Q_r and total heat flux including radiation Q_t are defined as:

$$Q_r=\left|\frac{Q_r|_{z=1}+Q_r|_{z=-1}}{2}\right|,$$
$$Q_r|_{z=\pm1}=\frac{1}{4N}\left|\int_{-A_2}^{A_2}\int_0^{A_1}q_r\,dx\,dy\right|_{z=\pm1} \tag{29}$$
$$Q_t=Q_r+Nu \tag{30}$$

The pressure boundary conditions are unknown. Many techniques have been devoted to determining the proper pressure boundary conditions [18–20]. Since the application of the continuity equation at the boundary allows any appropriate pressure field to satisfy the incompressibility constraint, time splitting techniques are introduced. Time splitting schemes are employed to determine the pressure field that provides a divergence-free velocity field at the end of each time step.

The time splitting method implemented in the spectral method was developed by Ku et al. [20] who applied the technique to a three-dimensional problem with three nonperiodic directions and a first-order time stepping scheme. However, explicit treatment of the diffusion terms imposes severe restrictions on the time increment. In the present calculations, a modified time splitting method [15] is introduced, which uses a second-order Adams–Bashforth (AB/2BE) time discretization [21]. In this procedure, the linear terms are treated implicitly to improve the numerical stability and the nonlinear terms are treated explicitly to avoid iterations. The advantage of the AB/2BE second-order scheme is that the momentum and energy equations take the form of Helmholtz equations, which can be solved efficiently using matrix diagonalization techniques.

To solve the resulting Helmholtz equations at each time step, a Fourier–Chebyshev collocation method is used [12]. For the periodic direction, physical variables are represented by truncated Fourier series expansions on a uniformly spaced grid. Truncated Chebyshev polynomial expansions are applied for the nonperiodic directions, using a Chebyshev–Gauss–Lobatto grid. This procedure results in a set of two-dimensional Helmholtz equations in coefficient space for each Fourier wave number. Further details of the procedures used can be found in Lan [15], Ku et al. [20], and Hill and Ball [22].

3. Results

3.1. Linear stability analysis

First, the convergence of the solution of the problem is examined by increasing the number of expansion terms. The critical Rayleigh numbers and the corresponding wave number in the case of a nonradiating fluid between two rigid surfaces have the exact values, 1707.76 and 3.117. As we increase the expansion order to over 10 terms of Chebyshev polynomials, the critical Rayleigh number and the corresponding wave number are the exact values shown in Fig. 2. For the case of a radiating source, 16 expansion terms are considered in the calculations.

Radiation provides an additional heat transfer mode to Rayleigh–Bénard convection, and the energy in the flow field can be released more efficiently than for single mode heat transfer. As a result, the flow is stabilized. To investigate radiation effects on the flow field, we study the particular case of $\tau_D^2/N=1$ by using two limiting formulations for the optical limits. Fig. 3 and Table 1 show that both limiting approaches overestimate the critical Rayleigh number.

Christophorides and Davis [3] studied the case of an optically thin medium using a simplified form of the reference state temperature gradient; Bdéoui and

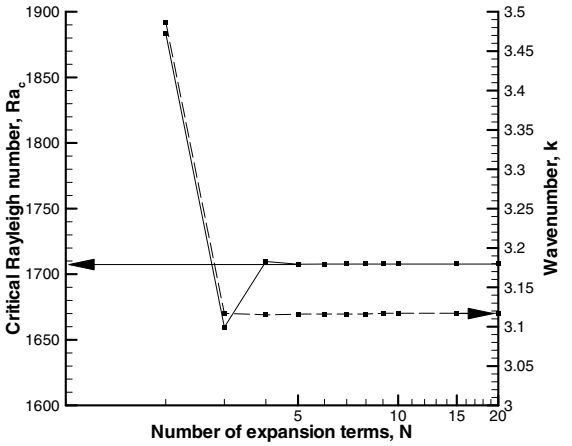

Fig. 2. The convergence of the truncation terms.

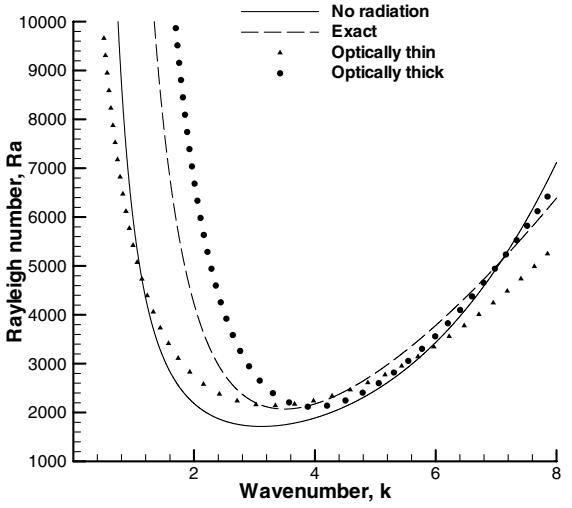

Fig. 3. The effect of optical thickness on the critical Rayleigh number for a gray gas between horizontal rigid boundaries for $\tau_D^2/N = 1$.

Soufiani [7] used the exact form of the reference state temperature gradient (Eq. (10)). Comparisons are made and shown in Table 2. The present results agree with those of Bdéoui and Soufiani [7].

Table 1
The predictions of critical Rayleigh number and critical wave number by linear stability theory

	Ra_c	k
No radiation	1707.62	3.117
$N = 1.0$, $\tau_D = 1.0$ (exact)	2071.47	3.356
$N = 1.0$, $\tau_D = 1.0$ (optically thick)	2114.51	3.970
$N = 1.0$, $\tau_D = 1.0$ (optically thin)	2143.03	3.332

As the optical thickness is increased, another asymptotic radiative limit may also be examined. Arpaci and Gozum [4] applied P–N approximations to the linear stability analysis of radiating Rayleigh–Bénard convection. The P–N method results slightly overestimated Ra_c, as shown in Fig. 4. In Fig. 4, increasing the optical thickness is predicted to stabilize the flow, and this is especially apparent for $\tau \geqslant 1$.

In the optically thin limit, the critical Rayleigh number reaches 1707.76 which is the exact value for pure natural convection. In the optically thick limit, the conventionally defined critical Rayleigh number asymptotically approaches a larger value as seen in Fig. 4.

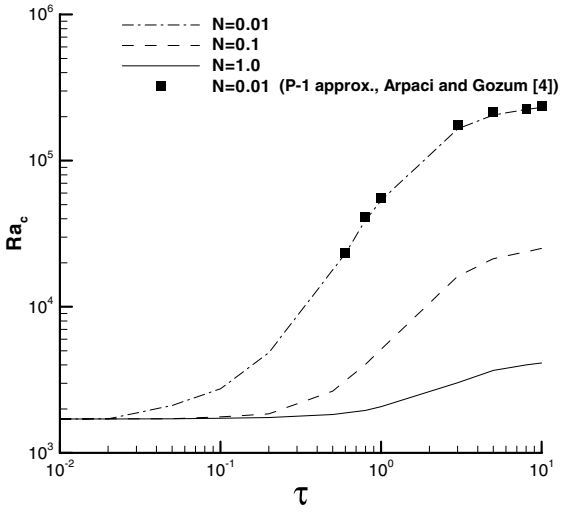

Fig. 4. The effect of N and optical thickness τ on the critical Rayleigh number for a gray gas with rigid boundaries.

Table 2
Comparisons of critical Rayleigh number and corresponding wave number

	$3\tau^2\chi$	Christophorides and Davis [3]		Bdéoui and Soufiani [7]		Present results	
		k	Ra_c	k	Ra_c	k	Ra_c
$\gamma = -0.5$	5	3.34	2127.42	3.33	2112.02	3.33	2112.10
$\gamma =$ exact	5	–	–	3.33	2358.03	3.356	2357.02

$\gamma = -dT/dz$, $\chi = 16\sigma\overline{T}^3/3a\kappa$.

To gain insight into this effect, it is useful to define a new Rayleigh number, Ra'_c based on an augmented thermal diffusivity $(\alpha_c + \alpha_r)$, where the radiative diffusivity $\alpha_r = k_r/\rho c$ (where κ_r is the equivalent radiative conductivity, $= 16\sigma\overline{T}^3/3a$) and α_c is the conventional diffusivity based on thermal conductivity;

$$Ra'_c = \frac{g\beta\Delta TL^3}{(\alpha_c + \alpha_r)v} \tag{31}$$

The ratio of Ra'_c to Ra_c is

$$\frac{Ra'_c}{Ra_c} = \frac{g\beta\Delta TL^3/(\alpha_c + \alpha_r)v}{g\beta\Delta TL^3/\alpha_c v} = \frac{\alpha_c}{(\alpha_c + \alpha_r)} = \frac{\kappa}{(\kappa + \kappa_r)} = \frac{\kappa}{\left(\kappa + \frac{16\sigma\overline{T}^3}{3a}\right)} = \frac{1}{\left(1 + \frac{4}{3N}\right)} \tag{32}$$

The new relationship for modified Rayleigh number vs. optical thickness is shown in Fig. 5. In the optically thick limit, the new critical Rayleigh numbers overshoot 1708, but become closer to 1708 as the conduction–radiation parameter (N) approaches to larger values. This further confirms the notion that radiative stability is generated by a radiatively diffusive process, particularly at large optical thickness.

The overshoot of the modified Ra'_c at large values of optical thickness τ occurs because of the use of the arithmetic mean reference temperature in the definition of the radiative diffusivity. A reference temperature based on the fourth-power mean would be more appropriate.

3.2. Direct numerical simulation of three-dimensional convection with radiation

All calculations start with small sinusoidal velocity perturbations in order to obtain the proper steady-state roll pattern. The modified time splitting method is applied to handle the unknown pressure boundaries and the medium domain is discretized by the Fourier–Chebyshev spectral collocation scheme. The reference temperature is 500 K, and temperature difference is $\Delta T/T = 0.05$. All calculations are performed on IBM RS/6000 43P-240 workstations. Each case consumes CPU time ranging from days to weeks depending on the grid size and time interval. Due to computational limitations, the conduction–radiation parameter (N) and optical thickness (τ_D) are set to be unity in all simulations. To find the corresponding critical Rayleigh number with the addition of radiation, the computation starts with $Ra = 3000$, which is assumed to be a supercritical value relative to the critical Rayleigh number for $\tau_D = N = 1.0$. Three different aspect ratio combinations are considered: (1) $A_1 = 2\pi$, $A_2 = 4$, (2) $A_1 = 10$, $A_2 = 10$, and (3) $A_1 = 20$, $A_2 = 10$.

In Fig. 6, a representative grid independence study is shown for the aspect ratio combination $A_1 = 2\pi$, $A_2 = 4$ with $Ra = 3000$ and $Pr = 0.71$, without radiative effects. The figure shows the mean square "error" of the dimensionless temperature and velocity components at different grid resolutions ranging from $16 \times 16 \times 16$ to $64 \times 64 \times 64$, using results with a grid resolution of $128 \times 128 \times 128$ to approximate the "true" solution.

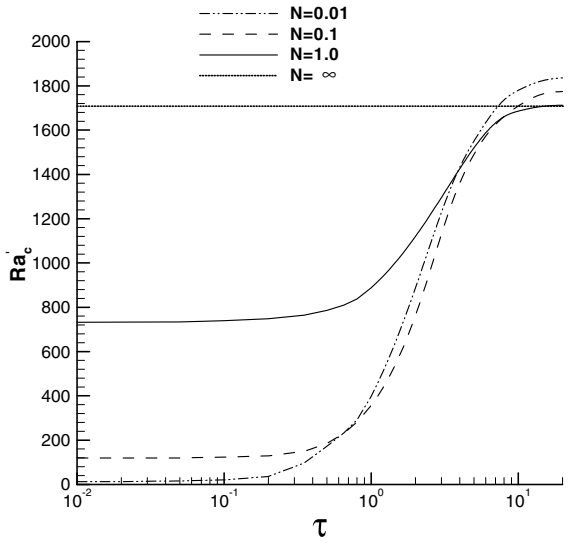

Fig. 5. The effect of N and optical thickness τ on the new critical Rayleigh number Ra'_c for gray gas with rigid boundaries.

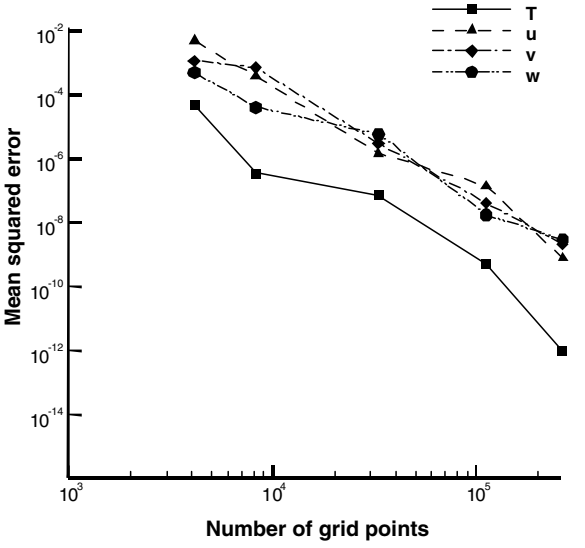

Fig. 6. The rate of convergence for the aspect ratios, $A_1 = 2\pi$, $A_2 = 4$, $Ra = 3000$, and $Pr = 0.71$.

Table 3
Thermophysical properties and radiative emittance for heteropolar gases for ($PL_e = 2$ atm ft, in Hottel chart [24]) total pressure $P = (1)$ 0.2 atm; (2) 1.0 atm; (3) 5.0 atm

	Temperature (K)	Pr	a (m^{-1})	Conduction–radiation, N		
				(1)	(2)	(3)
CO_2	800	0.716	0.185	1.56e−4	7.78e−4	3.89e−3
NH_3	580	0.817	0.70	4.73e−4	2.36e−3	1.18e−2

The temperature and velocity components are observed to be converging as the total number of grid points is increased, and a high level of accuracy is achieved with a $64 \times 64 \times 64$ grid (which is used for all results presented in this paper).

In practice, only heteropolar gases, such as CO_2, H_2O, CO, SO_2, NO, NH_3, and CH_4 absorb and emit significantly. Air is almost transparent to infrared radiation and does not emit significantly. Gases with $Pr \approx 0.71$ and high emittance or absorption coefficient are CO, CO_2, and NH_3. Table 3 shows the values from the thermophysical property tables [23] and emittance charts [24], which provide the appropriate values for the equivalent gray gases for our cases.

The steady-state roll patterns for the nonradiative flow and the flow combined with the effect of the radiative medium do not show any difference under the same conditions, but the amplitude of velocity components are different. Fig. 7 shows the steady-state velocity distribution for $Ra = 2500$, $Pr = 0.71$ and the aspect ratios of $A_1 = 2\pi$, $A_2 = 4$ for the nonradiative flow and the

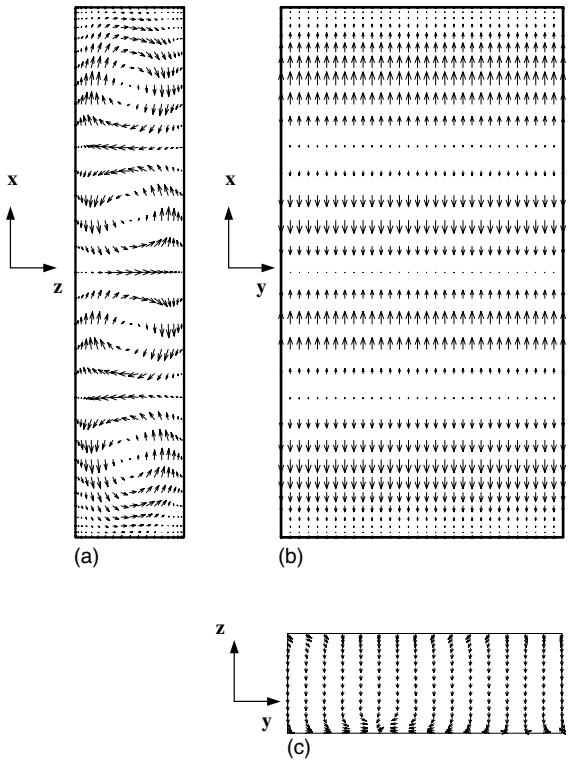

Fig. 7. Steady-state velocity distribution for $Ra = 2500$, $Pr = 0.71$ and aspect ratios $A_1 = 2\pi$, $A_2 = 4$ (a) (x,z)-plane at $y = 0.5A_2$; (b) $(x$–$y)$-plane at $z = 0.9$; (c) (y,z)-plane at $x = 0.1A_1$.

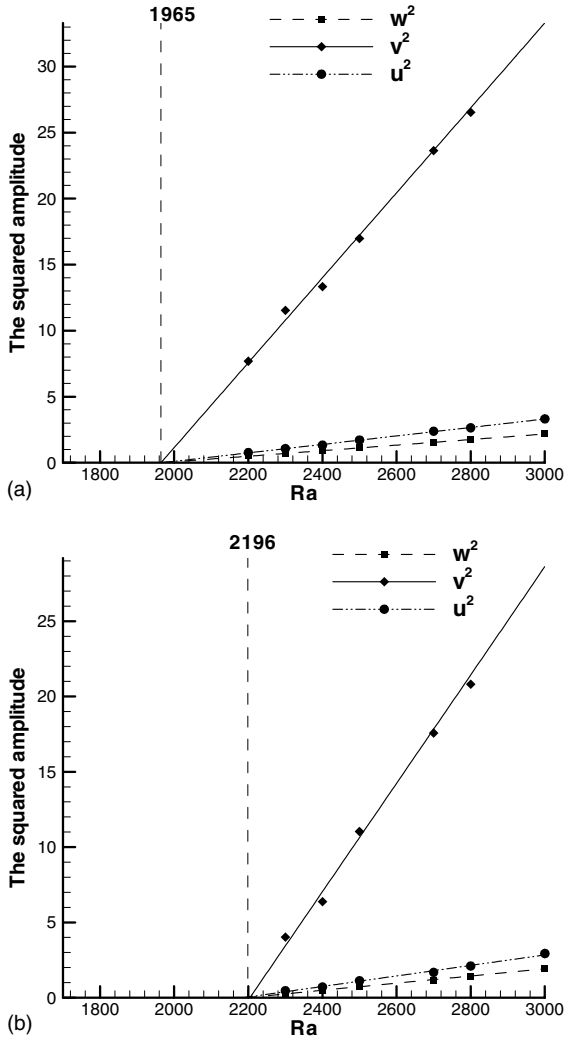

Fig. 8. Squared amplitude of the velocity components at a characteristic point for (a) pure natural convection (b) combined convection–radiation with $\tau_D/N = 1.0$ and aspect ratios $A_1 = 2\pi$, $A_2 = 4$.

flow combined with radiative medium. Four rolls with axes parallel to the y-direction occur in the enclosure. To indicate the critical Rayleigh number, bifurcation diagrams are made, which can predict the critical Rayleigh number by extrapolating the results obtained at supercritical values of Ra. A linear fit is applied to obtain the extrapolated critical Rayleigh values. In Fig. 8, the bifurcation diagram of squared amplitude of the velocity components at a characteristic point (0.392, 0.885, 0.115), shows that the extrapolated critical number Ra_c is 1965 for pure natural convection; for combined convection–radiation with $\tau_D = N = 1.0$, the extrapolated critical number, Ra_c is 2196. As Ra and Pr remain at the same values and the aspect ratios increase to $A_1 = A_2 = 10$, the steady-state roll patterns change to five symmetric cells distributed in the enclosure for the non-radiative flow and the flow combined with radiative medium, shown in Fig. 9. The phenomenon of change in steady-state roll patterns is investigated in many experimental studies, such as Stork and Müller [25], Maveety and Leith [10]. Neither study completely explains this behavior. In the Maveety and Leith [10] study, the authors demonstrated that the roll structures and the heat transport are strongly dependent on size and shape of the container. In Fig. 10, the bifurcation diagrams show that at location (1.95, 7.73, 0.329), the extrapolated critical number Ra_c predicted here is 1812 for pure natural convection; for combined convection–radiation with $\tau_D = N = 1.0$, the extrapolated critical number, Ra_c is 2102. Compared to the critical values of the smaller

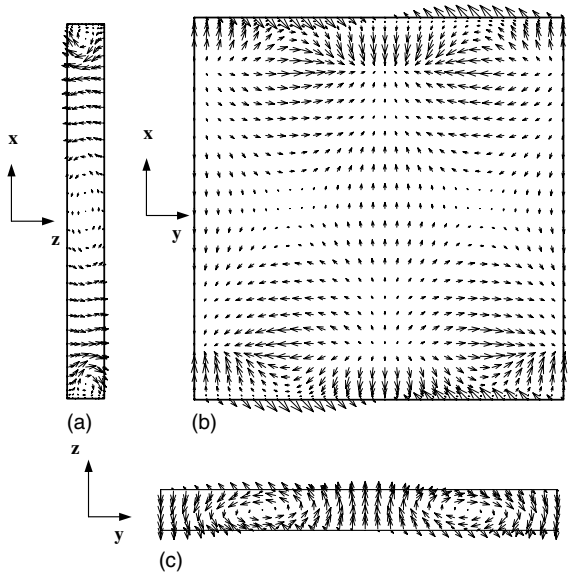

Fig. 9. Steady-state velocity distribution for $Ra = 2500$, $Pr = 0.71$ and aspect ratios $A_1 = 10$, $A_2 = 10$ (a) (x,z)-plane at $y = 0.75A_2$; (b) $(x$–$y)$-plane at $z = 0.9$; (c) (y,z)-plane at $x = 0.5A_1$.

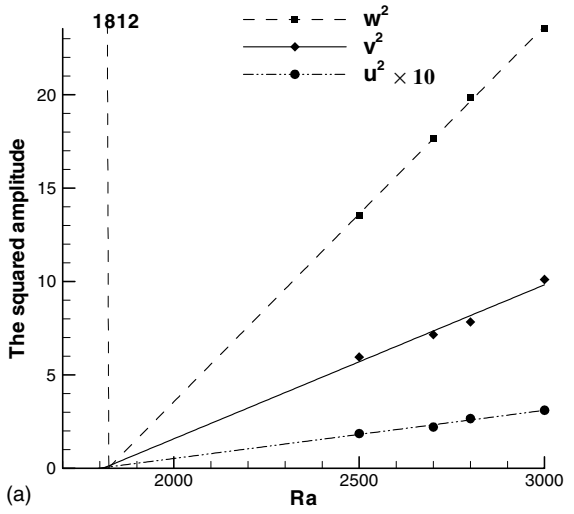

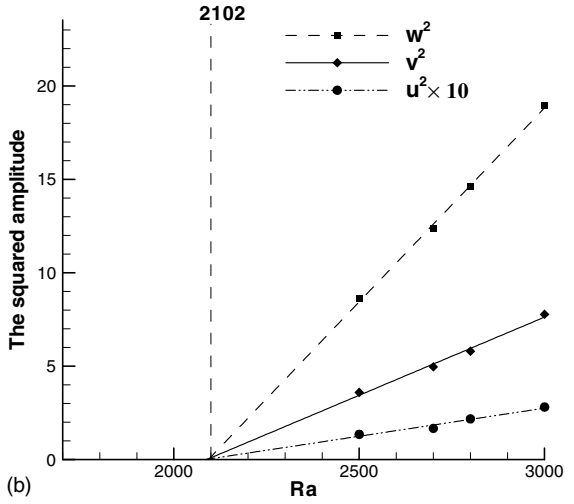

Fig. 10. Squared amplitude of the velocity components at a characteristic point for (a) pure natural convection (b) combined convection–radiation with $\tau_D/N = 1.0$ and aspect ratios $A_1 = A_2 = 10$.

aspect ratios, $A_1 = 2\pi$ and $A_2 = 4$, Ra_c decreases 4% for combined convection–radiation with $\tau_D = N = 1.0$ and decrease 7% for pure natural convection. The above results show that if the radiative heat transfer mode is introduced into the analysis of the system, then the critical Rayleigh number is increased, and the flow becomes more stable.

In Table 4, comparisons of the predicted critical Rayleigh numbers are made between the present work and others' experimental and numerical results for pure natural convection. The results show that the effect of

Table 4
Comparisons of critical Rayleigh numbers between linear stability results, numerical simulations, and experimental studies for pure natural convection

	Aspect ratios	*Pr*	Ra_c
Linear stability analysis			
Present	$A_1 = \infty$, $A_2 = \infty$	–	1707.76
Numerical simulations			
Kuo and Ball [26]	$A_1 = 4.0$, $A_2 = 2.0$	6.7	1934
Mukutmoni and Yang [27]	$A_1 = 4.0$, $A_2 = 2.0$	0.71	1950
Mukutmoni and Yang [29]	$A_1 = 2.42$, $A_2 = 1.2$	5.0	2420
Present	$A_1 = 2\pi$, $A_2 = 4.0$	0.71	1965
	$A_1 = 10.0$, $A_2 = 10.0$	0.71	1812
	$A_1 = 20.0$, $A_2 = 10.0$	0.71	1774
Bdéoui and Soufiani [7]	2-D ($A_1 = 15$, $A_2 = \infty$)	–	1690
		Medium	
Experimental studies			
Gille and Goody [8]	$A_1 = 10.0$, $A_2 = 10.0$	Air[a]	1786 ± 16
Hutchison and Richards [9]	$A_1 = 40.0$, $A_2 = 20.0$	Air[a]	1760 ± 70
Maveety and Leith [10]	$A_1 = 8.0$, $A_2 = 3.0$	Air[a]	1880
	$A_1 = 10.0$, $A_2 = 4.0$	Air[a]	1850
	$A_1 = 12.0$, $A_2 = 4.0$	Air[a]	1800
	$A_1 = 14.0$, $A_2 = 4.0$	Air[a]	1780
	$A_1 = 16.0$, $A_2 = 6.0$	Air[a]	1730

[a] $Pr = 0.707$–0.709.

the aspect ratios on critical values is large. Both numerical and experimental results show that the critical Rayleigh number decreases by increasing aspect ratios. The present numerical results for the aspect ratios of $A_1 = A_2 = 10$ find that the critical value is 1812, compared to the experimental results $Ra_c = 1786 \pm 16$ for the same aspect ratio by Gille and Goody [8]. The difference is less than 1.5%. Even though the difference is slightly out of the variation range, the result is still quite accurate. In the linear analysis, the linearized perturbation equations (19) and (20) which predict the critical Rayleigh number do not consider Prandtl number effects. Numerical calculations show that the effect of *Pr* number on critical values is very small. Kuo and Ball [26] used water ($Pr = 6.7$) for the aspect ratios $A_1 = 4$ and $A_2 = 2$, and obtained the critical Rayleigh number as 1934. Mukutmoni and Yang [27] used air ($Pr = 0.71$) for the same aspect ratios, and obtained a critical Rayleigh number of 1950. The difference between them is less than 1%.

In Table 5, comparisons of the predicted critical Rayleigh numbers are made between the present work and others' experimental and numerical results for combined convection and radiation. Comparisons of the weakly nonlinear stability analysis show that the present result, $Ra_c = 3133.58$ for $N = 0.1$, $\tau_D = 0.6$ has very good agreement with the predicted result by Bdéoui and Soufiani [7]. Numerical simulation results also show that the critical Rayleigh number decreases for increasing aspect ratios. However, the flow has different radiative properties, and the predicted critical values are quite different. The present numerical results for $Pr = 0.71$ and aspect ratios of $A_1 = A_2 = 10$, give a critical value of 2102, compared to the experimental results $Ra_c = 2125 \pm 93$ for the same aspect ratio but different medium (NH_3) performed by Gille and Goody [8]. The difference is about 1.1%.

Studies of radiative effects at different aspect ratio on the critical values are performed. The present linear stability analysis predicts Ra_c to decrease by 21% for $N = \tau_D = 1.0$ in the radiatively participating gas. In numerical simulations, the obtained critical Rayleigh numbers decrease 17.5%, 16%, and 12% for the aspect ratios of 20×10, 10×10, and $2\pi \times 4$, respectively. The trend shows that effects of the presence of a radiative source in the flow become more important as the aspect ratios increase, and the limit is 21% for $N = \tau_D = 1.0$.

In Table 6, heat transfer in Rayleigh–Bénard convection is investigated. The simplified correlation of Nusselt number for experimental results reported by Hollands et al. [28] is

$$Nu = 1 + 1.44\left(1 - \frac{1708}{Ra}\right) \quad 1708 < Ra < 5500 \qquad (33)$$

The present results of the average *Nu* for different Rayleigh numbers and the aspect ratios of 20×10 and the experimental results for the aspect ratios of 40×20 investigated by Hutchison and Richards [9] have very good agreement with Eq. (33) for pure natural convec-

Table 5
Comparison of critical Rayleigh numbers between linear stability results, numerical simulations, and experimental studies for combined convection–radiation

	Aspect ratios	Medium	Ra_c
Linear stability analysis			
Bdéoui and Soufiani [7]	$A_1=\infty, A_2=\infty$	Gray ($N=0.1, \tau_D=0.6$)	3133.66
	$A_1=\infty, A_2=\infty$	H_2O ($N=0.1, \tau_D=0.6$)	5232.24
Present	$A_1=\infty, A_2=\infty$	$N=0.1, \tau_D=0.6$	3133.58
	$A_1=\infty, A_2=\infty$	$N=1.0, \tau_D=1.0$	2071.47
Numerical simulations			
Bdéoui and Soufiani [7]	2-D ($A_1=15, A_2=\infty$)	Gray ($N=0.1, \tau_D=0.6$)	3080
	2-D ($A_1=15, A_2=\infty$)	H_2O ($N=0.1, \tau_D=0.6$)	5426
Present	$A_1=2\pi, A_2=4.0$	$N=\tau_D=1$, $Pr=0.71$	2196
	$A_1=10.0, A_2=10.0$	$N=\tau_D=1$, $Pr=0.71$	2102
	$A_1=20.0, A_2=10.0$	$N=\tau_D=1$, $Pr=0.71$	2084
Experimental studies			
Gille and Goody [8]	$A_1=10.0, A_2=10.0$	NH_3[a] ($N=2.4\times10^{-3}, \tau_D=8\times10^{-2}, Pr=0.87$)	2125 ± 93
Hutchison and Richards [9]	$A_1=40.0, A_2=20.0$	(CO_2 + air)	1830 ± 100
	$A_1=40.0, A_2=20.0$	CO_2[a] ($N=7.8\times10^{-4}, \tau_D=2\times10^{-3}, Pr=0.725$)	2050 ± 90

[a] Values are estimated from the thermophysical property tables for pure components.

Table 6
Comparisons of Nusselt numbers and nondimensional heat flux between numerical simulations, experimental results, and correlation equation for pure convection and combined convection–radiation

Ra		Hollands et al. [28] Eq. (33)	Hutchison and Richards [9] ($A_1=40.0$, $A_2=20.0$)		Present ($A_1=2\pi$, $A_2=4.0$)		Present ($A_1=10.0$, $A_2=10.0$)		Present ($A_1=20.0$, $A_2=10.0$)	
			Air	CO_2	(no rad.)	$N=\tau_D=1.0$	(no rad.)	$N=\tau_D=1.0$	(no rad.)	$N=\tau_D=1.0$
3000	*Nu*	1.62	1.63[a]	1.35[a]	1.895	1.583	1.758	1.471	1.616(0.2%)	1.347(0.2%)
	$\lvert Q_r\rvert$	–	–	–	–	0.392	–	0.407	–	0.423
	$\lvert Q_t\rvert$	–	–	–	1.895	1.975	1.758	1.878	1.616	1.770
2800	*Nu*	1.56	1.55[a]	1.28[a]	1.796	1.476	1.674	1.389	1.548(0.8%)	1.274(0.4%)
	$\lvert Q_r\rvert$	–	–	–	–	0.388	–	0.403	–	0.416
	$\lvert Q_t\rvert$	–	–	–	1.796	1.864	1.674	1.792	1.548	1.690
2500	*Nu*	1.46	1.45[a]	1.21[a]	1.701	1.363	1.581	1.281	1.451(0.6%)	1.194(1.3%)
	$\lvert Q_r\rvert$	–	–	–	–	0.380	–	0.396	–	0.408
	$\lvert Q_t\rvert$	–	–	–	1.701	1.773	1.581	1.677	1.451	1.602

[a] Interpolated values.

tion. The differences are less than 1%. For the radiatively participating media, the present result of the average *Nu* for the aspect ratios of 20×10 also agree with the experimental results. In addition to the average *Nu*, the nondimensional radiative heat flux is considered in the present work. The results show that the nondimensional radiative heat flux is increased by increasing the aspect ratios. In contrast to the nondimensional radiative heat flux, the average total heat fluxes and the average Nusselt numbers are decreased by increasing the aspect ratios. The observed results strongly support the observation that the effects of additional radiative sources in the flow are increased as the aspect ratios increase.

4. Conclusion

In this study, one-dimensional linear stability analysis and three-dimensional direct numerical simulations based on spectral methods are used to examine the stability of combined radiation with natural convection heat transfer. The results show very good agreement with the existing numerical and experimental results.

The effect of radiative transfer on Rayleigh–Bénard convection is to stabilize the flow field. Basically, increasing the radiation effect in the participating fluid, by increasing the optical thickness or the conduction–radiation parameter, increases the stability of the fluid to perturbations. In the optically thin limit, conductive transfer dominates stability. Increasing the radiative effects results in increasing the temperature gradient in the participating medium and causes stabilization. In the optically thick limit, radiative transfer dominates the medium. Radiation provides a new mechanism affecting the onset of Rayleigh–Bénard convection. The calculations suggest that a modified Rayleigh number can be defined using the sum of the molecular diffusivity plus the radiative diffusivity in the denominator. The new critical Rayleigh number varies with the conduction–radiation parameter: decreasing N decreases its value. For optically thick media, the critical Rayleigh number including the effect of radiation may be predicted from Eq. (32) using $Ra'_c = 1708$. The present direct numerical simulations support the linear analysis theory. Additionally, the simulations demonstrate that the effects of the presence of the radiative source in the flow become stronger as the aspect ratios increase, and the limit is $(Ra_{cr} - Ra_c)/Ra_c \times 100\% = 21.3\%$ for $N = \tau_D = 1.0$. It is also concluded that the critical Ra_c is increased by adding the radiative effect, and the flow is therefore stabilized by the presence of the radiative source.

Acknowledgements

C.H.L. would like to express his deepest appreciation to Dr. Dah-Chyi Kuo for his valuable help and guidance in the use of spectral techniques, making it possible to include many of the topics in this study.

References

[1] R.M. Goody, The influence of radiative transfer on cellular convection, J. Fluid Mech. 1 (1956) 424–435.
[2] E.A. Spiegel, The convective instability of a radiating fluid layer, Astrophys. J. 132 (1960) 716–728.
[3] C. Christophorides, S.H. Davis, Thermal instability with radiative transfer, Phys. Fluids 13 (1970) 222–226.
[4] V.S. Arpaci, D. Gozum, Thermal stability of radiating fluids: the Bénard problem, Phys. Fluids 16 (1973) 581–588.
[5] J.H. Lienhard V, Thermal radiation in Rayleigh–Bénard instability, J. Heat Transfer 112 (1990) 100–109.
[6] W.M. Yang, Effect of modulation on radiation-induced instability, Int. J. Heat Mass Transfer 38 (1995) 47–53.
[7] F. Bdéoui, A. Soufiani, The onset of Rayleigh–Bénard instability in molecular radiating gases, Phys. Fluids 9 (1997) 3858–3872.
[8] J. Gille, R. Goody, Convection in a radiating gas, J. Fluid Mech. 20 (1964) 47–79.
[9] J.E. Hutchison, R.F. Richards, Effect of nongray gas radiation on thermal stability in carbon dioxide, J. Thermophys. Heat Transfer 13 (1999) 25–32.
[10] J.G. Maveety, J.R. Leith, Heat transfer in Rayleigh–Bénard convection with air in moderate size containers, Int. J. Heat Mass Transfer 41 (1998) 785–796.
[11] A.J. Chorin, Numerical solution of the Navier–Stokes equations, Math. Comput. 22 (1968) 745–762.
[12] C. Canuto, M.Y. Hussaini, A. Quarterini, T.A. Zang, in: Spectral Methods in Fluid Dynamics, first ed., Springer-Verlag, New York, 1988, pp. 31–75.
[13] D.C. Kuo, J.C. Morales, K.S. Ball, Combined natural convection and volumetric radiation in a horizontal annulus: spectral and finite volume predictions, J. Heat Transfer 121 (1999) 610–615.
[14] D.B. Haidvogel, T.A. Zang, The accurate solution of Poisson's equation by expansion in Chebyshev polynomials, J. Comput. Phys. 30 (1979) 167–180.
[15] C.H. Lan, Radiative combined-mode heat transfer in a multi-dimensional participating medium using spectral methods, Ph.D. dissertation, The University of Texas at Austin, Texas, 2000.
[16] R. Siegel, J.R. Howell, in: Thermal Radiation Heat Transfer, fourth ed., Taylor and Francis, Washington, 2002, pp. 565–571.
[17] S. Chandrasekhar, Hydrodynamic and Hydromagnetic Stability, Oxford University Press, Oxford, 1961.
[18] S.A. Orszag, D. Gottlieb, High resolution spectral calculations of inviscid compressible flows, in: Approximation Methods for Navier–Stokes Problems, Springer, New York, 1980, pp. 381–398.
[19] P. Moin, J. Kim, On the numerical solution of time-dependent viscous incompressible fluid flows involving solid boundaries, J. Comput. Phys. 35 (1980) 381–392.
[20] H.C. Ku, R.S. Hirsh, T.D. Taylor, A pseudospectral method for solution of the three-dimensional incompressible Navier–Stokes equations, J. Comput. Phys. 70 (1987) 439–462.
[21] U. Ehrenstien, R. Peyret, A Chebyshev-collocation method for the Navier–Stokes equations with application to double-diffusive convection, Int. J. Numer. Meth. Fluids 9 (1989) 427–452.
[22] R. Hill, K.S. Ball, Parallel implementation of a Fourier–Chebyshev collocation method for incompressible fluid flow and heat transfer, Numer. Heat Transfer, Part B 36 (1999) 309–329.
[23] F.P. Incropera, D.P. DeWitt, in: Fundamentals of Heat and Mass Transfer, fourth ed., John Wiley & Sons, New York, 1996, pp. 839–843.
[24] H.C. Hottel, A.F. Sarofim, Radiative Transfer, McGraw-Hill, New York, 1967.
[25] K. Stork, U. Müller, Convection in boxes: experiments, J. Fluid Mech. 54 (1972) 599–611.
[26] D.C. Kuo, K.S. Ball, Essential differences between Boussinesq and variable density simulations of bifurcations in Rayleigh–Bénard convection, in: H. Bau, L.A. Bertram, S.A. Korpela (Eds.), Bifurcation Phenomena and Chaos in Thermal Convection ASME HTD 214, 1992, pp. 25–32.

[27] D. Mukutmoni, K.T. Yang, Pattern selection for Rayleigh–Bénard convection in intermediate aspect ratio boxes, Numer. Heat Transfer, Part A 27 (1995) 621–637.
[28] K.G.T. Hollands, G.D. Raithby, L. Konicek, Correlation equations for free convection heat transfer in horizonal layers of air and water, Int. J. Heat Mass Transfer 18 (1975) 879–884.
[29] D. Mukutmoni, K.T. Yang, Thermal convection in small enclosures: an atypical bifurcation sequence, Int. J. Heat Mass Transfer 38 (1995) 113–126.